Solvent Reorganization Energy and Free Energy Change for Donor/Acceptor Electron Transfer at Micelle Surfaces: Theory and Experiment

H. L. Tavernier,[†] A. V. Barzykin,[‡] M. Tachiya,[‡] and M. D. Fayer*,[†]

Department of Chemistry, Stanford University, Stanford, California 94305, and Department of Physical Chemistry, National Institute of Materials and Chemical Research, Tsukuba, Ibaraki 305, Japan

Received: April 7, 1998

Theories are presented for calculating the solvent reorganization energy and the free energy change which occur in photoinduced donor/acceptor electron transfer at the surface of micelles. The theories are based on the Marcus theory for spherical reactants in a dielectric continuum. The micelle is modeled with regions of differing dielectric properties, representing the micelle core, the headgroup region, and the surrounding water. The free energy change accompanying electron transfer can be calculated from redox measurements made in bulk liquids. The theories are applied to previously published photoinduced intermolecular electron-transfer data between octadecylrhodamine B (ODRB) and *N*,*N*-dimethylaniline (DMA) molecules.[1] The ODRB and DMA molecules are located in the surface region of three different types of surfactant micelles: dodecyl-, tetradecyl-, and cetyl-trimethylammonium bromide (DTAB, TTAB, and CTAB, respectively). The data show an increased rate of electron transfer with increasing micelle radius. Application of the new theory to the electron-transfer data along with information provided by neutron scattering experiments show that the headgroup regions of the three micelles have different dielectric constants because water penetration into the headgroup regions decreases as the surfactant length increases.

I. Introduction

Photoinduced electron transfer is influenced substantially by the local environment of the donor and acceptor. The form of this dependence has been of considerable interest for many years.[2−6] Solvents will affect diffusion rates, free energies of transfer (ΔG), and solvent reorganization energies (λ). Theories have been developed for calculating these quantities in bulk liquid solvents.[2,7,8] However, electron transfer dynamics in heterogeneous restricted geometry systems can differ markedly from those in bulk solvents. Restricted geometry systems are of interest because of their potential to prolong the lifetime of charge transfer states, a goal of electron-transfer studies interested in solar energy utilization.[9−13] Theories developed for use in bulk solvent systems are not expected to apply to systems of different geometry. For a donor interacting with many acceptors all undergoing spatial diffusion, the geometry of the system determines the time-dependent distribution of donor/acceptor distances, which profoundly affects the time dependence of photoinduced electron transfer. For example, electron transfer from a donor to acceptors confined to move on the surface of spherical micelles has been studied theoretically and experimentally.[1,14−16] The electron transfer dynamics are substantially modified by the restricted distribution of separations arising from the spherical geometry of the system, compared to those in a homogeneous liquid.

In addition to strictly geometrical changes in distance distributions, it has been recognized that heterogeneous restricted geometry systems can have an impact on the solvent reorganization energy, and solvent reorganization energies have been calculated for some restricted geometry systems.[5,17] In addition, the free energy change associated with electron transfer is modified by a heterogeneous environment. This paper addresses photoinduced electron transfer for donors and acceptors on the surface of spherical micelles. In particular, the natures of the reorganization energy and the free energy are examined both theoretically and experimentally. The Marcus and Rehm−Weller forms for these quantities were derived for spherical reactants in a dielectric continuum.[2,8] For donors/acceptors confined to the headgroup region of a micelle, the environment is far from a dielectric continuum. The headgroup region has dielectric properties that are distinct from the interior of the micelle, and both the headgroup region and the interior of the micelle dielectric properties differ substantially from the bulk water which surrounds the headgroup region. Both the reorganization energy and the free energy are modified by the micelle's three-"layer" system, and both are sensitive to the properties of each layer.

The sheer magnitude of literature concerning micelles demonstrates their importance and complexity. Micelles have been studied by techniques such as NMR,[18,19] X-ray scattering,[20,21] neutron scattering,[22] light scattering,[23,24] cryo-transmission electron microscopy (TEM),[25,26] molecular dynamics simulations,[27,28] and Monte Carlo simulations.[29] In addition to their important biological and industrial applications, micelles have long been of interest to the electron-transfer community.[1,9,16,30−36] Despite this substantial attention, surprisingly little is known experimentally about the characteristics of micelles' surface regions.

Micelles formed near the critical micelle concentration from ionic surfactants with fairly short tails are essentially spherical (see Figure 1A).[37,38] Their cores consist of the surfactant molecules' hydrocarbon tails and have approximately the density of pure hydrocarbon.[28,37] Outside this core is a complex headgroup region. If the surfactant molecules are ionic, this headgroup region contains ionic headgroups, counterions, water,

[†] Stanford University.
[‡] National Institute of Materials and Chemical Research.

S1089-5647(98)01754-4 CCC: $15.00
Published on Web 07/10/1998

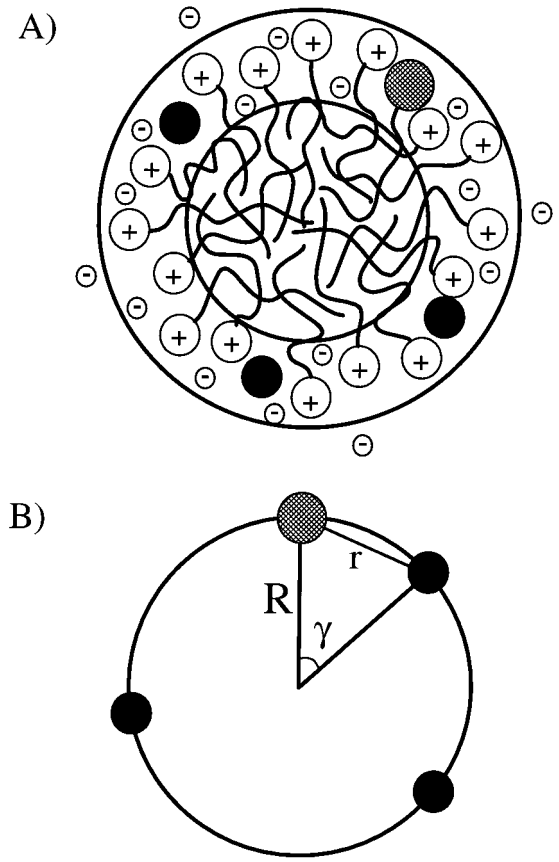

Figure 1. (A) Schematic diagram of a micelle, indicating three regions. The region inside the smaller circle contains the surfactant tails and is the hydrocarbon core. The region outside the largest circle is water with counterions. The shell between the two circles is the region of surfactant headgroups ("+"), most of the counterions ("−"), the donor (hatched) and acceptor (solid) molecules, portions of the surfactants' hydrocarbon tails, and some water. The dielectric properties of this region are expected to be intermediate between those of water and hydrocarbon. (B) A diagram showing the geometry used in the calculations. Donor (hatched) and acceptor (solid) molecules are shown as spheres on the surface of a larger sphere. R is the distance between the center of the micelle and the donor/acceptor molecules, r is the distance between the donor and an acceptor. γ is the angle between the lines joining the center with the donor and an acceptor. γ can be used to obtain the cord length, r.

and portions of the surfactants' hydrocarbon tails that have water molecules associated with them.[20,37,39−43] The headgroup region forms a shell around the micelle's core, and the entire entity is surrounded by water and possibly some counterions that are not bound closely to the headgroup region.[42,43] Although this model of a micelle is fairly well accepted,[39] the literature varies from treating micelles as uniform spheres[25,44] to treating them as two regions, with the width of the headgroup region comparable to the radius of the core region.[27,41] Whether this surface region is wide enough to have its own set of distinct properties, what governs diffusive motion within this shell, and how this environment affects intermolecular electron transfer are a few of the questions still under active investigation.

This paper introduces a new theory for calculating the solvent reorganization energy for molecules confined to the headgroup region of micelles. A corresponding theory for calculating the free energy of electron transfer is presented, in which ΔG on a micelle surface can be calculated from quantities measured in bulk liquids. The theories are applied to photoinduced intermolecular electron-transfer data between octadecylrhodamine B (ODRB) and *N*,*N*-dimethylaniline (DMA) molecules.[1] The

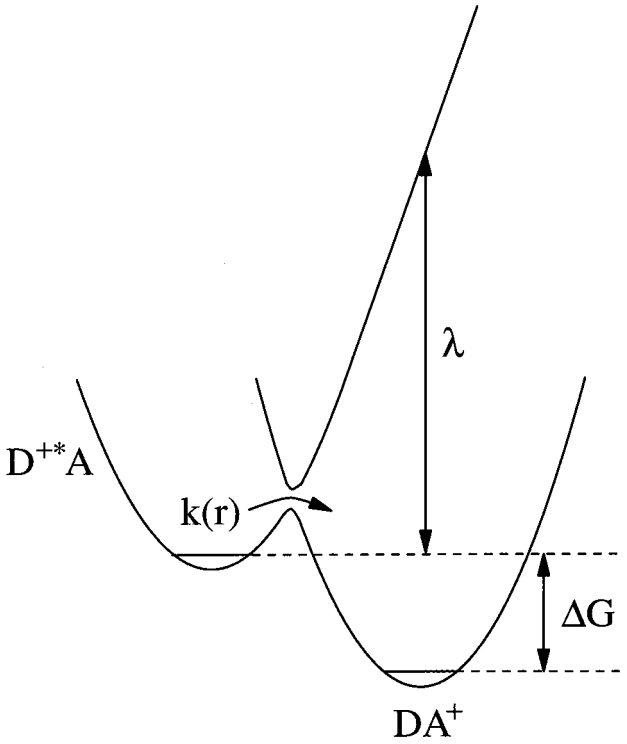

Figure 2. Free energy diagram showing reactant and product states of the system. Reactants include the photoexcited donor and neutral acceptor (D^{+}*A). Population can leave the excited state by either fluorescence ($1/\tau$) or electron transfer ($k(r)$) to create the charge-transfer products (DA^{+}). The solvent reorganization energy (λ) and free energy of forward transfer (ΔG) are indicated. The x-axis denotes reaction coordinate.

ODRB and DMA molecules are located in the surface region of three different types of surfactant micelles: dodecyl-, tetradecyl-, and cetyl-trimethylammonium bromide (DTAB, TTAB, and CTAB, respectively). Time-resolved fluorescence and fluorescence yield data reveal an increasing rate of electron transfer with increasing micelle radius. Utilization of the theories results in successful fits of the data. The micelle size dependence of the electron-transfer rate arises because the dielectric constant in the headgroup region varies with micelle size. The results, along with information provided by neutron scattering experiments,[22,42] show that the headgroup regions of the three micelles have different dielectric constants because water penetration into the headgroup regions decreases as the surfactant length increases.

II. Theory

Each micelle contains at most one donor molecule, which is photoexcited and exchanges an electron with any one of a number of acceptors on the same micelle. The electron-transfer process can be modeled by a two-state potential well system (see Figure 2). The ground state donor−acceptor system is photoexcited with a laser pulse. In the case shown, the photoexcited donor (D) begins as a positive ion and the acceptor (A) begins as neutral, to correspond to the experimental system described later. This excited state is depleted by two competing processes: relaxation to the ground state, with rate $1/\tau$, and electron transfer, with distance-dependent rate $k(r)$. ($k(r)$ is the rate of forward electron transfer, which is treated here. The combined problem of forward electron transfer and geminate recombination has been studied.[45−48] The same considerations that are treated here for forward transfer apply to the distance-dependent back transfer rate.)

The form developed by Marcus in the 1950s for the distance-dependent rate coefficient for nonadiabatic electron transfer in the normal regime has been proven to be accurate in a wide variety of systems.[49,50] For the type of micelle systems under consideration here, the Marcus transfer rate can be written as a function of γ:[2,3,51]

$$k(\gamma) = \frac{2\pi}{\hbar} J^2 \exp\left[-2R\beta\left(\sin\left(\frac{\gamma}{2}\right) - \sin\left(\frac{\gamma_o}{2}\right)\right)\right] \frac{1}{\sqrt{4\pi k_B T}} \times \exp\left[\frac{-(\Delta G + \lambda)^2}{4\lambda k_B T}\right] \quad (1)$$

where γ is the angle between the lines joining the donor and acceptor molecules on the micelle surface to the micelle center (Figure 1B). γ_o, which accounts for donor−acceptor excluded volume, is the angle at which the donor and acceptor hard spheres are in contact. R is the distance between the centers of the micelle and the donor/acceptor molecules, $\hbar$ is Planck's constant, k_B is Boltzmann's constant, and T is temperature. J is the contact value of the donor/acceptor electronic coupling, β characterizes the distance dependence of the electronic coupling, λ is the solvent reorganization energy, and ΔG is the free energy change of transfer.

The rate of electron transfer depends on many factors, including the identity of the donor/acceptor, energies of solvation and ionization, and distances. The solvent reorganization energy, λ, is the energy required to have solvent molecules in position to solvate the charge-transfer state but without charge-transfer having occurred (see Figure 2). ΔG is the free energy difference between the reactant and charge-transfer states (see Figure 2). The rate of transfer is also a function of r, the center-to-center distance between donor and acceptor molecules. On the micelle, distances can be written in terms of angle γ: $r = 2R\sin(\gamma/2)$, where r is the intermolecular distance and R is the distance between the centers of the micelle and the donor/acceptor molecules (see Figure 1B). In the analysis of the distance dependence of the transfer rate, R is taken to be a constant, determined by the micelle size. Then γ fully characterizes the distance between the donor and acceptor on the surface of a micelle of given radius.

Marcus derived a form of λ for spherical reagents in a dielectric continuum,[2,3,51] and Rehm and Weller derived a form of ΔG for similar conditions.[8] However, neither is directly applicable to the problem of electron transfer on the surface of a micelle.

A. Reorganization Energy. According to Marcus, the outer sphere reorganization energy depends on the size of reactants and the separation distance, as well as on the dielectric properties of the embedding solvent. In his original formulation, a homogeneous solution was considered. Thus, to describe the electron transfer data on micelle surfaces, we have to properly account for heterogeneous local structure of micelles.

We start with a model for which we neglect all the charges except those participating in the electron-transfer event, although the system consists of charged micelles surrounded by a sea of counterions. However, it has been conjectured in the literature that the effect of small ionic species should be modest compared with the orientational reorganization energy of polar solvent molecules.[52] The role of the charged headgroups and counterions will be treated in a subsequent study.

The dielectric spherical shell model of a micelle used for the calculations is shown in Figure 3B. We represent a micelle as a sphere with dielectric properties different from those of the external solvent. The interfacial headgroup area, where the reactants are located, is modeled by a concentric shell with its own dielectric parameters. The reactants are also assumed to be spherical. a_C is the radius of the micelle core. a_S is a_C plus the thickness of the headgroup shell. a_D is the radius of the donor, and a_A is the radius of the acceptor. The donor and acceptor are required to be completely enclosed by the shell region so that $a_S \geq a_C + 2\max(a_D, a_A)$. R_D is the distance from the center of the micelle to the center of the donor, and R_A is the distance from the center of the micelle to the center of the acceptor. For numerical calculations, we will take $R = R_D = R_A = a_C + \max(a_D, a_A)$. However, this condition is not used in the derivation. Finally, r is the distance between the donor/acceptor centers.

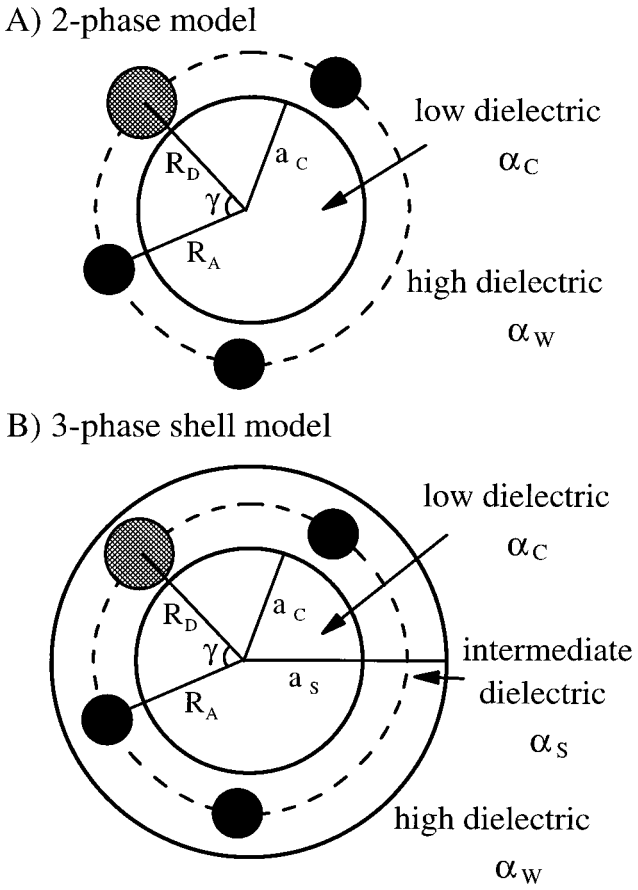

Figure 3. (A) 2-phase model for the micelle system. The interior of the micelle is taken to be a sphere of radius a_C with hydrocarbon dielectric properties. The medium outside this core is assumed to have the dielectric properties of water. The donor (hatched) and acceptor (solid) molecules, with radii a_D and a_A, lie outside the micelle core at distances R_D and R_A from the center of the micelle. (B) 3-phase model. Again, the interior of the micelle is taken to have a low static dielectric constant. The donor and acceptor molecules are located in a shell of radius a_S which surrounds the micelle core. This shell contains not only the donor and acceptor molecules but also the surfactant headgroups, counterions, portions of the surfactant hydrocarbon tails, and water (see Figure 1A). It is assumed to have a static dielectric constant between that of hydrocarbon and water. Finally, the shell is surrounded by water.

We follow the dielectric continuum approach,[2,3,51] and thus adopt all of the ensuing assumptions. The solvent reorganization energy is given by

$$\lambda = \sum_q \frac{e^2 \alpha_q}{32\pi^2 \epsilon_o} \int (\mathbf{E}_D - \mathbf{E}_A)^2 \, dV \quad (2)$$

where $\alpha_q = \epsilon_{op,q}^{-1} - \epsilon_{st,q}^{-1}$. q = C, S, or W to refer to the micelle core, headgroup shell, or water region surrounding the micelle, respectively. e is the charge of an electron, ϵ_o is the permittivity of free space. $\epsilon_{op,q}$ and $\epsilon_{st,q}$ denote the optical and static dielectric permittivities of the appropriate region. $\mathbf{E}_D$ and $\mathbf{E}_A$ are the vectors of electric displacement determined by the total charge distribution on the donor and the acceptor, respectively. The integration is performed over all of the space excluding the two cavities, D and A. We assume the reactants to be conducting particles and neglect the contribution of the induced charges. In general, the Laplace (Poisson) equation can be solved for the electrostatic potential satisfying the appropriate boundary conditions to determine the electric induction vectors (and the corresponding displacement). To simplify the problem, we follow the approach of Marcus[2] and assume that the electric induction can be approximated by the associated electric field due to a given charge distribution in a vacuum,

$$\mathbf{E}_p(\mathbf{r}) = -\nabla|\mathbf{r} - \mathbf{r}_p|^{-1} \tag{3}$$

where p = D or A.

With the above assumption, the integration in eq 2 can be carried out analytically. It is convenient to rewrite λ as follows:

$$\lambda = \lambda_0 + \lambda_1 + \lambda_2 \tag{4}$$

where

$$\lambda_0 = \frac{e^2\alpha_S}{32\pi^2\epsilon_o}\int_{\infty-v_D-v_A}(\mathbf{E}_D - \mathbf{E}_A)^2\,dV = \frac{e^2\alpha_S}{8\pi\epsilon_o}(I_1 - I_{21}) \tag{5}$$

$$\lambda_1 = \frac{e^2(\alpha_C - \alpha_S)}{32\pi^2\epsilon_o}\int_{v_C}(\mathbf{E}_D - \mathbf{E}_A)^2\,dV = \frac{e^2(\alpha_C - \alpha_S)}{8\pi\epsilon_o}[I_{22}(a_C) - I_3(\rho(a_C), \gamma)] \tag{6}$$

$$\lambda_2 = \frac{e^2(\alpha_W - \alpha_S)}{32\pi^2\epsilon_o}\int_{\infty-v_S-v_C}(\mathbf{E}_D - \mathbf{E}_A)^2\,dV = \frac{e^2(\alpha_S - \alpha_W)}{8\pi\epsilon_o}[I_{22}(a_S) - I_3(\rho(a_S), \gamma)] \tag{7}$$

where v_q values denote the volumes of the appropriate micelle regions and reactants, $\rho(a_q) = a_q/(R_D R_A)^{1/2}$, and the integrals, I, are defined below.

λ_0 is the reorganization energy that would apply if the electron transfer occurred in a bulk liquid with the dielectric properties of the headgroup shell region, with

$$I_1 = \frac{1}{4\pi}\int_{\infty-v_D}\mathbf{E}_D{}^2 dV + \frac{1}{4\pi}\int_{\infty-v_A}\mathbf{E}_A{}^2 dV - \frac{1}{2\pi}\int_{\infty-v_D-v_A}\mathbf{E}_D\mathbf{E}_A\,dV = \frac{1}{a_D} + \frac{1}{a_A} - \frac{2}{r} \tag{8}$$

being the main Marcus term and

$$I_{21} = \frac{1}{4\pi}\int_{v_A}\mathbf{E}_D{}^2\,dV + \frac{1}{4\pi}\int_{v_D}\mathbf{E}_A{}^2\,dV = f(r,a_A) + f(r,a_D) \tag{9}$$

the Kharkats correction,[53] where

$$f(r,a_q) = \frac{a_q}{2|r^2 - a_q{}^2|} - \frac{r - a_q}{4r|r - a_q|}\ln\frac{r + a_q}{|r - a_q|} \tag{10}$$

λ_1 defines the correction due to the micelle core. Such three-center correction terms have been calculated previously.[54] Thus we have,

$$I_{22}(a_q) = \frac{1}{4\pi}\int_{v_q}(\mathbf{E}_D{}^2 + \mathbf{E}_A{}^2)dV = f(R_D, a_q) + f(R_A, a_q) \tag{11}$$

and

$$I_3(\rho(a_q), \gamma) = \frac{1}{2\pi}\int_{v_q}\mathbf{E}_D\mathbf{E}_A\,dV = \frac{1}{\sqrt{R_D R_A}}\sum_{n=0}^{\infty}\left(1 \mp \frac{1}{2n+1}\right)\rho^{\pm(2n+1)}P_n(\cos\gamma) \tag{12}$$

where $P_n(x)$ denote Legendre polynomials, and the upper sign corresponds to $\rho(a_q) < 1$, the case for λ_1. The lower sign applies for the calculation of λ_2. λ_2 corrects for the external solvent. Because we neglected the effect of induced charges, the approximate expression obtained is universal and applicable to both charge separation and charge shift reactions. The identical approach can be applied to the problem of geminate recombination. Among the contributions to the reorganization energy, $(e^2/8\pi\epsilon_0)\alpha_S I_1$ is the Marcus term, and the modifications arising from the system's heterogeneity are determined by the terms with I_{22} and I_3.

The reorganization energy for the 2-phase model (see Figure 3A), in which the micelle's headgroup region is not treated as distinct from the surrounding water, has already been calculated[54] and is equal to

$$\lambda = \lambda_0 + \lambda_1 \tag{13}$$

where α_S is replaced by α_W.

B. Free Energy. The free energy change of photoinduced electron transfer can be written:[55]

$$\Delta G(r) = IP_D - EA_A - W_r + W_p - h\nu \tag{14}$$

where IP_D is the ionization potential of the donor, EA_A is the electron affinity of the acceptor, $W_{r/p}$ values denote the total energy change to bring the reactants/products together on a micelle surface at the given separation distance, h is Planck's constant, and ν is the frequency at which the donor's normalized absorption and fluorescence spectra cross.[50]

Weller calculated ΔG in a bulk solvent with a known static dielectric constant when redox potentials are known in a solvent with a different static dielectric constant.[56] Following his method, ΔG on the surface of a micelle can be calculated from oxidation−reduction potentials measured in bulk solution. The ionization potential of the donor and the electron affinity of the acceptor can be written in terms of donor/acceptor oxidation/reduction potentials ($E^{ox/red}$) and solvation free energies as follows:

$$IP_D - EA_A = (E_D{}^{ox} - E_A{}^{red})_B + \left(1 - \frac{1}{\epsilon_B}\right)(S_p - S_r) \tag{15}$$

where B denotes measurements made in a bulk liquid with static

dielectric constant ϵ_B. The redox term for bulk solution can be measured experimentally with cyclic voltammetry. $S_{r/p}$ is the solvation energy of individual reactant/product ions in a vacuum:

$$S = \frac{e^2}{8\pi\epsilon_o}\left(\frac{{q_D}^2}{a_D} + \frac{{q_A}^2}{a_A}\right) \quad (16)$$

where q_D and q_A are the charges (in units of e) on the donor/acceptor. Reactant charges should be used for calculation of S_r and product charges should be used for calculation of S_p. Solvation energies calculated in this section assume a reference state of infinitely separated reactants/products in vacuum. $IP_D - EA_A$ can be equated for the micelle and bulk liquid systems because it is a relation of gas-phase properties.

$W_{r/p}$ terms incorporate both solvation energies and Coulomb interactions of the ions. They can be written as:

$$W = \frac{e^2}{32\pi^2\epsilon_o}\left[\frac{1}{\epsilon_S}\int_{\infty-\upsilon_A-\upsilon_D} + \left(\frac{1}{\epsilon_C} - \frac{1}{\epsilon_S}\right)\int_{\upsilon_C} + \left(\frac{1}{\epsilon_W} - \frac{1}{\epsilon_S}\right)\int_{\infty-\upsilon_S-\upsilon_C}\right] \times (q_D\mathbf{E}_D + q_A\mathbf{E}_A)^2\, dV - S \quad (17)$$

where $\mathbf{E}_D$ and $\mathbf{E}_A$ are given by eq 3, and ϵ_C, ϵ_S, and ϵ_W are the static dielectric constants for the micelle core, shell, and water, respectively. Reactant and product charges are used for W_r and W_p, respectively. The integrals can be calculated using eqs 8−12 from the previous section.

ΔG for the 3-phase micelle system can be calculated by substituting eqs 15−17 into eq 14. The result is valid in both charge separation and charge shift cases for any reactant/product charges. The experimental system considered in sections III and IV of this paper is a case of charge shift: $D^+A \rightarrow DA^+$. The final equation for this case can be simplified because reactants are assumed to be equidistant from the micelle center and thus the integrals over υ_C and $\infty-\upsilon_S-\upsilon_C$ are zero. The final result for charge shift in a micelle is:

$$\Delta G = (E^{ox} - E^{red})_B + \frac{e^2}{8\pi\epsilon_o}\left(\frac{1}{\epsilon_S} - \frac{1}{\epsilon_B}\right)\left(\frac{1}{a_A} - \frac{1}{a_D} + f(r,a_A) - f(r,a_D)\right) - h\nu \quad (18)$$

For the case of charge separation, the presence of the micelle can influence the free energy of electron-transfer significantly. However, the theory shows that for charge shift, $D^+A \rightarrow DA^+$, there is no micelle size dependence in ΔG. In fact, the calculation of ΔG in this case is identical to the calculation necessary if the transfer were occurring in a bulk liquid with the static dielectric constant of the headgroup region, ϵ_S.

For the 2-phase model, in which the micelle's headgroup region is assumed to have the same properties as the surrounding water, the free energy is given by eqs 14−18, with ϵ_S replaced by ϵ_W.

The Rehm−Weller expression for ΔG in a bulk liquid[8] can be obtained by replacing ϵ_W, ϵ_S, and ϵ_C with ϵ_B in eqs 14−17 to obtain:

$$\Delta G = (E^{ox} - E^{red})_B + \frac{e^2(q_{Dp}q_{Ap} - q_{Dr}q_{Ar})}{4\pi\epsilon_o\epsilon_B r} - h\nu \quad (19)$$

where the Kharkats correction terms are neglected.

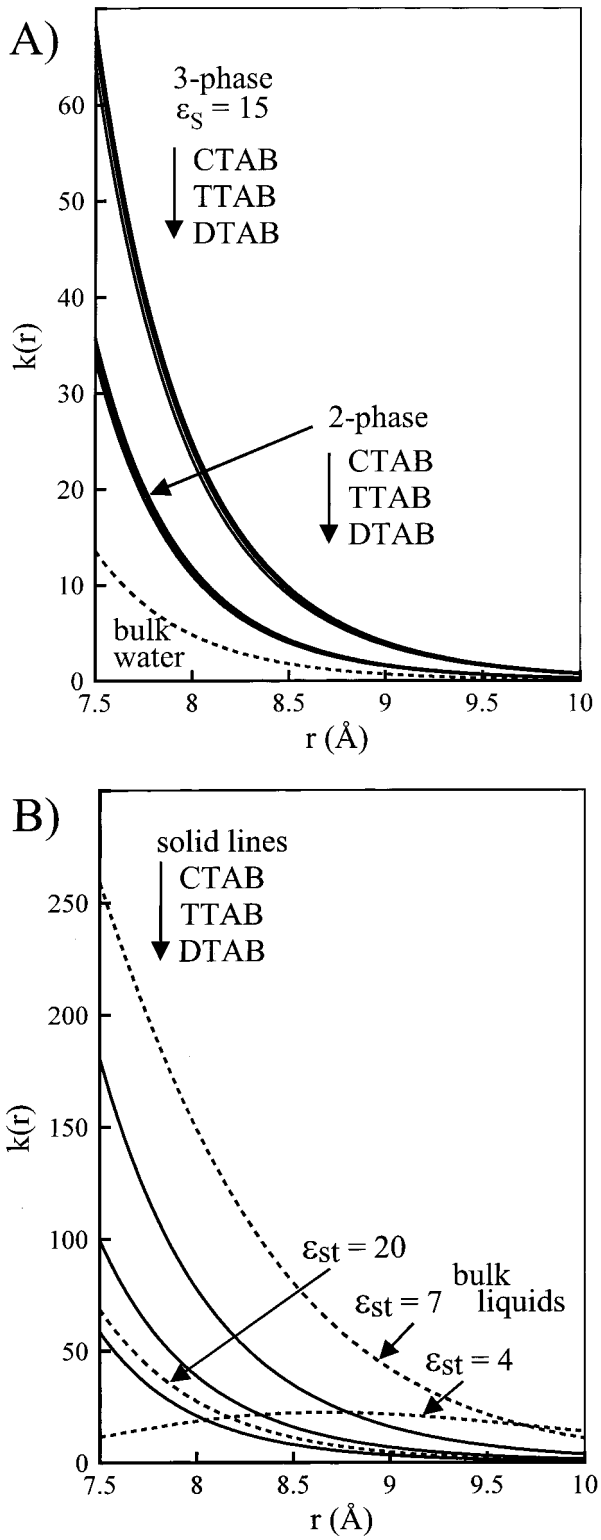

Figure 4. Plots of rate coefficient vs distance. (A) $k(r)$ is calculated both for bulk water (dashed line) and for the 2-phase and 3-phase micelle models (solid lines) for the three different micelle sizes given in Table 1. This plot shows that the reorganization energy is significantly different in the micelle models compared to bulk water and that the 3-phase model is notably different from the 2-phase model. Also, effects due purely to micelle size are not substantial. (B) Rate constants for bulk liquids with $\epsilon_{st} = 20$, 7, and 4 (dashed lines) are compared to rate constants for the micelle 3-phase model (solid lines). $k(r)$ is calculated for the micelles using micelle radii shown in Table 1 and $\epsilon_{st} = 20$, 7, and 4 in the shell region, corresponding to the final fits for electron-transfer data taken in DTAB, TTAB, and CTAB, respectively. The plots show that using the appropriate λ and ΔG for a micelle makes a significant difference in the rate coefficient.

TABLE 1

	R	ϵ_S in shell	J (cm^{-1})	D (Å^2/ns)
DTAB	16.7	20	30	4
TTAB	19.2	7	30	6
CTAB	21.7	4	30	7

C. Effect on Distance-Dependent Transfer Rate. Figure 4 shows plots of the distance-dependent rate coefficient for both bulk liquid and micelle cases. Although it is more convenient to write k as a function of γ for micelle calculations, the figure shows k as a function of r to more readily compare micelles to each other and to bulk liquids. r and γ are related by the micelle radius, R: $r = 2R\sin(\gamma/2)$. Figure 4A compares $k(r)$ for bulk water to $k(r)$ for the 2-phase and 3-phase micelle calculations for the three different micelle radii given in Table 1. $k(r)$ for the micelle calculations is determined using the forms of λ and ΔG given in eqs 13 and 18 ($\epsilon_S = \epsilon_W$, 2-phase model) and eqs 4 and 18 (3-phase model). The 2-phase model assumes that the micelle is basically a sphere of hydrocarbon surrounded by a water-like environment (see Figure 3A). The donor/acceptor are at the hydrocarbon core/water interface. The 3-phase model includes the headgroup shell (see Figure 3B). In the 3-phase model, the donor/acceptor are located in the headgroup shell. $\epsilon_{st} = 15$ was chosen to approximate the intermediate-dielectric properties of the headgroup shell region. The plots show that the distance-dependent rate coefficient is strongly influenced by the heterogeneous micelle environment. In the 2-phase model, even though the donor/acceptor are exposed to water, the plot demonstrates that inclusion of the hydrocarbon spherical core makes a substantial contribution to the character of $k(r)$. The 3-phase calculations demonstrate that $k(r)$ is further influenced by the headgroup shell. The plots also show that the changes in the rate coefficient due purely to changes in micelle radii are not significant for the radii that correspond to the micelles used in the experimental study. Therefore, although treating λ and ΔG properly has a significant effect on the calculated distance-dependent electron-transfer rate, the weak dependence on size is insufficient to explain the data reported previously.[1] The data are discussed below in light of the new theoretical considerations.

Figure 4B shows the rate coefficient vs distance for the final fits to the data using the 3-phase micelle model (see section IV). In these fits, the core and water dielectric constants are fixed, and the dielectric constant of the headgroup region is varied to fit the data in a consistent manner. In addition, plots of $k(r)$ are shown for bulk liquids with static dielectric constants matching those used for the headgroup region in micelle calculations. These plots show that the distance-dependent rates are, in fact, very different in the three types of micelles (see below). In addition, the figure shows that using the same headgroup region dielectric constants in the conventional isotropic theory produces wildly different distance-dependent rate coefficients than those of the 3-phase micelle theory. Thus, including the appropriate forms of λ and ΔG for the micelle is necessary to obtain the correct rate parameters.

D. Calculation of Observables. The physical quantity of interest in the experiments described here is $P_{ex}(t)$, the probability that the donor is in its excited state as a function of time after photoexcitation. Details of the derivations of the following equations have been published previously.[1,14,15] Although the equations in refs 14 and 15 are applicable for the model discussed here and for electron transfer in the presence of a potential of mean force, they are not valid in the presence of an arbitrary potential. Consequently, the equations given here are slightly different and are valid in the presence of any potential. A detailed account of analogous modifications for electron transfer in a dielectric continuum can be found in the appendix of ref 45. Diffusion and the rate of forward transfer are accounted for in the differential equation for the Green's function $G_{ex}(\gamma,t|\gamma_i)$:[57]

$$\frac{\partial}{\partial t}G_{ex}(\gamma,t|\gamma_i) = D\nabla_\gamma^2 G_{ex}(\gamma,t|\gamma_i) - k_f(\gamma)G_{ex}(\gamma,t|\gamma_i)$$

$$G_{ex}(\gamma,0|\gamma_i) = \frac{\delta(\gamma-\gamma_i)}{\pi R^2 \sin\gamma(1+\cos\gamma_o)} \qquad (20)$$

$$2\pi R^2 \sin\gamma_o D\frac{\partial}{\partial\gamma}G_{ex}(\gamma,t|\gamma_i)|_{\gamma=\gamma_o} = 0$$

where the diffusion operator is

$$D\nabla_\gamma^2 = \frac{D}{R^2\sin\gamma}\frac{\partial}{\partial\gamma}\left[\sin\gamma\frac{\partial}{\partial\gamma}\right]$$

and D is the sum of the donor and acceptor lateral diffusion coefficients. γ_o is the angle at which the donor and acceptor hard spheres are in contact. $G_{ex}(\gamma,t|\gamma_i)$ considers only the one-donor/one-acceptor case. It is the probability per unit area that at time t the donor is still excited and that the acceptor is at γ, given that the acceptor was located at γ_i at time 0. $G_{ex}(\gamma,t|\gamma_i)$ can be integrated over initial positions to get $S_{ex}(\gamma,t)$:

$$S_{ex}(\gamma,t) = \int_{\gamma_i} G_{ex}(\gamma,t|\gamma_i)\frac{2\pi R^2\sin\gamma_i}{4\pi R^2}\,d\gamma_i \qquad (21)$$

$S_{ex}(\gamma,t)$ is the probability per unit area that a donor is still excited at time t and that the acceptor is at γ for the one-donor/one-acceptor problem. $S_{ex}(\gamma,t)$ is the solution to a differential equation analogous to that in eq 20, with initial and reflecting boundary conditions as follows:

$$\frac{\partial}{\partial t}S_{ex}(\gamma,t) = D\nabla_\gamma^2 S_{ex}(\gamma,t) - k_f(\gamma)S_{ex}(\gamma,t)$$

$$S_{ex}(\gamma,0) = \frac{1}{2\pi R^2(1+\cos\gamma_o)} \qquad (22)$$

$$2\pi R^2\sin\gamma_o D\frac{\partial}{\partial\gamma}S_{ex}(\gamma,t)|_{\gamma=\gamma_o} = 0$$

The configuration average of the excited-state survival probability in a micelle with n acceptors is

$$\langle P_{ex}(t)\rangle_n = e^{-t/\tau}\left[\int_{\gamma_o}^{\pi} S_{ex}(\gamma,t)2\pi R^2\sin\gamma\,d\gamma\right]^n \qquad (23)$$

where τ is the fluorescence lifetime of the donor molecules in the absence of electron transfer. To get the final experimentally observable quantity, eq 23 must be combined with the fact that acceptor molecules are not distributed uniformly among micelles. Acceptor molecules are assumed to follow a Poisson distribution about N, the mean number of acceptors per micelle. Then, the observable, $\langle P_{ex}(t)\rangle$, is:

$$\langle P_{ex}(t)\rangle = \sum_{n=0}^{\infty}\frac{e^{-N}N^n}{n!}\langle P_{ex}(t)\rangle_n \qquad (24)$$

where $\langle P_{ex}(t)\rangle$ is independent of donor concentration because the concentration is low enough that each micelle has at most one donor.

Finally, fluorescence yield experiments measure the ratio, Φ, of the steady-state fluorescence for a sample with acceptors compared to that with no acceptors. The fluorescence yield can be expressed as

$$\Phi = \frac{\int_0^\infty \langle P_{ex}(t)\rangle dt}{\tau} \tag{25}$$

Φ is useful because it is not dependent on the shape of $\langle P_{ex}(t)\rangle$, but only on the integrated area of $\langle P_{ex}(t)\rangle$. In an experimental measurement of the time-dependent fluorescence, the observable is $\langle P_{ex}(t)\rangle$ convolved with the instrument response. Therefore, the short time behavior of $\langle P_{ex}(t)\rangle$ is lost in the convolution. Because Φ does not involve an instrument response, a simultaneous fit of Φ and the convolved $\langle P_{ex}(t)\rangle$ greatly narrows the range of parameters that are consistent with the data and yields parameters that properly describe the short time electron-transfer behavior. Data are fit to eqs 24 and 25 simultaneously, with a χ^2 fitting routine based on a downhill simplex method.[58,59]

III. Experimental Systems

Details of the sample preparation and experimental setup are given in ref 1. Briefly, the samples are aqueous solutions of micelles containing donor and acceptor molecules. Three types of micelles are used: DTAB, TTAB, and CTAB. Surfactant concentrations are near their respective critical micelle concentrations so that micelles formed are spherical and monodisperse.[1,20,25,26,38]

ODRB in its ground state is a singly charged positive ion with an 18-carbon chain that tethers it into the micelle so that the rhodamine B portion is in the headgroup region of the micelle.[60] ODRB is the molecule which is photoexcited, and its concentration is low enough that there is at most one ODRB molecule per micelle. For consistency with the terminology used in the theory, ODRB will be referred to as the donor, even though it is a "hole" donor.

DMA molecules are the hole acceptors. For each type of micelle, several samples were made, each with a different DMA concentration. The DMA molecules are assumed to follow a Poisson distribution with an average number N per micelle. Concentration can be characterized by the DMA packing fraction, η, which is defined as the percentage of the surface area of the micelle occupied by N DMA molecules (see ref 1). NMR experiments show that the DMA molecules are located in the headgroup region of the micelles (ref 1 includes a detailed verification of this point).[18,61]

R is the distance from the center of the micelle to the center of the donor/acceptor molecule. R, given in Table 1, is calculated for each micelle using the Tanford equation, $R = 1.5\ \text{Å} + 1.265\ \text{Å}\cdot T$, where T is the number of carbons in the hydrocarbon tail.[1,62] Donor and acceptor radii were determined from molecular modeling and from crystallographic data on similar compounds, using a technique described in detail previously.[63] The ODRB and DMA radii are 4.45 and 3.05 Å, respectively. γ_o varies with R and is the angle associated with the contact distance, 7.50 Å. The difference between oxidation and reduction potentials of the donor/acceptor species, ($E_D^{ox} - E_A^{red}$), was measured by cyclic voltammetry to be 1.6 eV in bulk acetonitrile ($\epsilon_{st} = 37$). Reference 1 includes details of the cyclic voltammetry. The excitation wavelength, ν, used to calculate ΔG, is 579 nm, the frequency at which normalized ODRB absorption and fluorescence spectra cross.[50]

Two types of fluorescence data were collected: time-dependent fluorescence decays and fluorescence yield. Time-dependent data were taken with the fluorescence upconversion technique. A 568 nm laser pulse is used to excite the sample. The fluorescence is gathered and focused into a nonlinear optical crystal, where it is mixed with another time-delayed laser pulse. The sum frequency light generated from the mixing is detected as a function of delay of the second pulse. The result is a time-dependent fluorescence decay. τ, the fluorescence lifetime of ODRB without acceptors present, was measured to be 1.8 ns in all three types of micelle solutions. Fluorescence yield measurements are corrected for ODRB concentration and compared to fluorescence from a sample containing no acceptors. In both types of fluorescence experiments, detection was done at the magic angle to eliminate contributions from orientational relaxation. All experiments were conducted at room temperature. Details of these experiments can be found in ref 1.

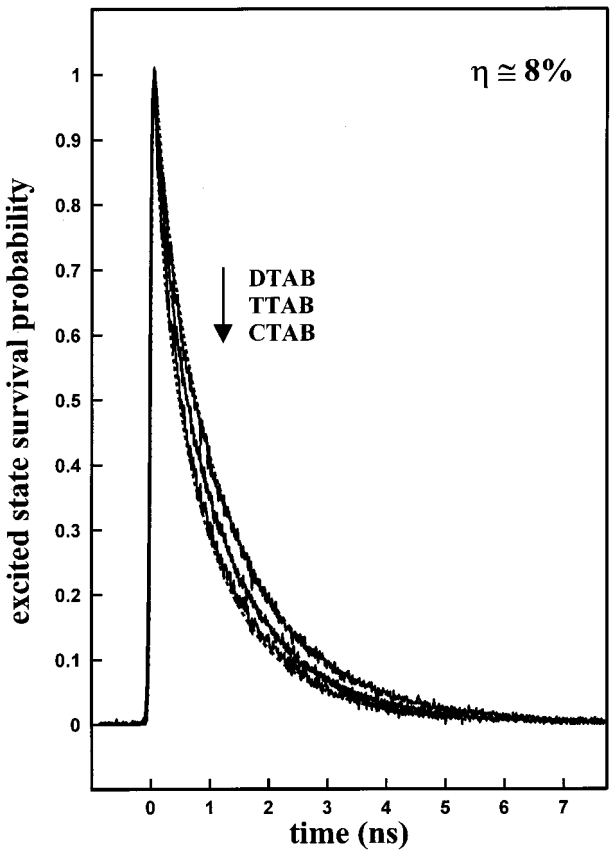

Figure 5. Examples of excited state survival probability data (solid lines) and fits (dashed lines) for all three micelles with approximately 8% packing fraction of DMA. The figure shows that the electron-transfer rate increases with micelle radius. Fits are almost indistinguishable from the data. Fits shown are for parameters given in Table 1.

IV. Experimental Results and Theoretical Analysis

Data on photoinduced intermolecular electron transfer between ODRB and DMA in micelles display a remarkable trend. Because the three micelles studied are so similar, it would be expected that for a given DMA packing fraction, the rate of transfer would be constant from one micelle to the next. Figure 5 shows $\langle P_{ex}(t)\rangle$ data for the almost identical DMA packing fractions ($\eta \approx 8\%$) in the three different micelles studied. The figure shows that the rate of electron transfer increases as the micelle size increases. Small differences in packing fraction are not enough to account for the differences in shape. In addition, plots of fluorescence yield vs η and the time for the

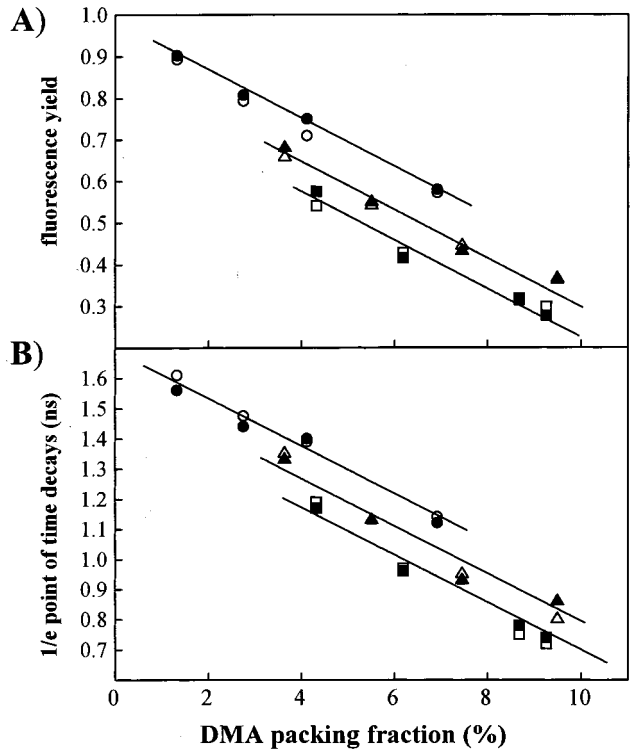

Figure 6. (A) Fluorescence yield data (solid) and fits (outlines) as a function of DMA packing fraction for DTAB (circles), TTAB (triangles), and CTAB (squares). Fits shown are for parameters given in Table 1. (B) 1/*e* point of time-dependent fluorescence data curves vs packing fraction. Although the decays are not exponential, this plot demonstrates the differences between the decays in the different micelle systems. Lines are guides to the eye. Although the trends are somewhat linear in this region, theory shows that as packing fraction approaches 0, the fluorescence yield values approach 1 in a nonlinear fashion.

fluorescence decay to fall to 1/*e* vs η display the same trends (See Figure 6). The lines in the figures are guides to the eye. Figure 6A shows that fluorescence yield is not dependent solely on DMA packing fraction. Although the data are not exponential, the plot of 1/*e* time (Figure 6B) provides a measure of the relative rates of decay in the various samples. For a given packing fraction the fluorescence decays faster as the micelle size increases.

Independent of any theoretical model, Figure 6 demonstrates that the excited-state survival probability depends on the size of the micelle. Because the excited-state lifetimes are identical in the three micelles, the differences in survival probability arise from differences in electron-transfer dynamics. The electron transfer theory presented in section II was applied to the data to determine the source of the observed differences. First, the original theory, which accounts for the micelle's geometry-imposed distribution of donor/acceptor distances but treats λ and ΔG with the homogeneous model, was applied. Parameters resulting from the fits to the data with the theory provide insights into the causes of the observed micelle size-dependent electron-transfer dynamics. In the fits, D and J were allowed to vary. Many electron-transfer studies have found $\beta \cong 1.0$ Å^{-1} (see discussion in ref 1).[64−68] Because fits are not strongly dependent on β, β was held fixed at this value. ΔG was calculated using the Rehm−Weller equation (eq 19) using the value of ($E_D^{ox} - E_A^{red}$) for acetonitrile and dropping the coulomb terms because there is no coulomb interaction between the experimental donor/acceptor pair. The Marcus continuum form for λ, which can be obtained by removing I_{21} from eq 5, was used with the dielectric constants for water, $\epsilon_{op} = 1.77$, $\epsilon_{st} = 78.3$.[69] The theory can distinguish between the effects of diffusion and the rate constant.

Fits using this model are similar in quality to those presented in Figure 5. The fits are nearly indistinguishable from the data in all three curves and for data obtained over a wide range of packing fractions. Consistent fits are obtained for each type of micelle over the full range of packing fractions. The resulting parameters are $J = 50$, 100, and 190 cm^{-1}, and $D = 5$, 6, and 7 Å^2/ns, for DTAB, TTAB, and CTAB, respectively. Diffusion constants in this range are consistent with experiments on diffusion in micelles.[32,70−72] Although diffusion has a notable effect on the electron-transfer process,[15,32,70−72] the differences in the diffusion constants obtained from the fits are not large enough to account for the observed differences in transfer dynamics. However, the fits produce significantly different J values for the three types of micelles.[1] By varying J, the distance-dependent transfer rate is varied. J depends primarily on the identity of the donor and acceptor species. It is the value of the donor−acceptor electronic coupling matrix element at the contact distance. J should not depend strongly on the molecules' environment, and the headgroup regions of the three micelles are very similar. The fact that very different J values are necessary to fit the data suggests that the variation in J is a surrogate for factors that have not been included in the theoretical treatment. It is reasonable to assume that, in fact, the J values should be essentially identical, and another factor is responsible for the variation of the electron-transfer dynamics with micelle size.

In ref 1, all possible explanations of the size-dependent data were examined in great detail within a context in which λ and ΔG were treated using the homogeneous model. It was found that the size dependence could not be explained. However, the data could be fit with very similar J values when the Marcus distance-dependent form of λ is arbitrarily multiplied by a different constant for each micelle. This fitting procedure demonstrated that the essence of the size dependence is contained in the λ dependence of the distance-dependent transfer rate, but such a qualitative approach does not provide a method to obtain a quantitative description of the role of λ and ΔG in electron transfer in the heterogeneous micelle system.

To obtain a quantitative understanding of the data, λ and ΔG were calculated with the 2-phase model for electron transfer on the surface of micelles. The micelle is modeled by a sphere of low dielectric with the donor and acceptor at the water interface and surrounded by the higher dielectric (water) continuum (see Figure 3A). This simple model assumes that the headgroup region has dielectric properties which are essentially those of water. Donors and acceptors are still expected to reside near the headgroups, where the outermost methylene groups are, so R values are the same as those used in the previous section (see Table 1). Some water is expected to be associated with the first few methylene groups of the surfactants, so the radius of the pure hydrocarbon core will be smaller than R. For the purposes of calculation, the donor and acceptor must be completely outside the low-dielectric region. To fulfill this requirement, we let $a_C = R - 4.45$ Å, where a_C is the radius of the micelle core and 4.45 Å is the larger of the donor/acceptor radii. This number is perhaps smaller than one would predict, but it is not more than 20% different than the average radius measured for the core of DTAB, TTAB, and CTAB in neutron scattering experiments.[22,42] In the hydrocarbon core, dielectric constants are taken to be those of hexane, $\epsilon_{op} = \epsilon_{st} = 1.88$.[69] Dielectric constants used for the water region are $\epsilon_{op} = 1.77$, $\epsilon_{st} = 78.3$.[69] λ and ΔG were calculated from

eqs 13 and 18 ($\epsilon_S = \epsilon_W$), respectively, using parameters given in Section III. Excellent fits to the data were achieved using the 2-phase model with parameters $J = 40$, 60, and 120 cm^{-1}, and $D = 4$, 6, and 7 $Å^2$/ns. Although the values for J are somewhat closer to each other than for the continuum model, the differences in the J values are still substantial and still do not seem physically reasonable. Variation in the size chosen for the core does not substantially influence the results. The 2-phase model is not sufficient to account for the physical properties of the micelle samples.

The failure of the 2-phase model occurs because a hydrocarbon core surrounded by water is not a realistic description of the micelles. Micelles have a layer surrounding the hydrocarbon core that has properties between those of hydrocarbon and water (see Figure 3B). This region contains the micelle headgroups, counterions, water, and methylene groups that have water molecules associated with them (see Figure 1A). From Monte Carlo and molecular dynamics simulations and from neutron scattering and X-ray scattering data on micelles, it is known that this shell on surfactant micelles with small, ionic headgroups is 5−9 Å thick.[20,22,27,29,41,42] For the calculations, we require the donor and acceptor to be completely enclosed in the intermediate-dielectric region. Therefore, because the diameter of the donor is 8.9 Å, and we do not expect the shell to be any larger than this, the shell is assumed to be this width. $a_C = R - 4.45$ Å, as it is for the 2-phase model. $a_S = R + 4.45$ Å, where a_S is the outer radius of the intermediate-dielectric spherical shell. Changing the shell width by ±10% results in less than 10% change in the J values, and no change in D values resulting from fits. Therefore some error in shell width does not substantially change the results of the calculations. In addition, a small error in donor/acceptor radii will affect the J and D values resulting from fits. However, using varying values of ODRB/DMA radii results in similar changes in J for all three micelle systems, and therefore does not affect the results discussed below. Dielectric constants for the core and for the water region are the same as in the 2-phase model. The optical dielectric constant of the shell region does not affect fits significantly, so $\epsilon_{op} = 1.88$ was chosen.

A range of values of the static dielectric constant in the headgroup region, ϵ_S, were used for each type of micelle. λ and ΔG were calculated from eqs 4 and 18, using the parameters given in section III. Using the 3-phase model, parameters were varied to find fits to both time-dependent fluorescence and quantum yield data for all three micelles that would result in the same J value for all three micelles. The resulting fits are shown in Figures 5 and 6. The fits are excellent, nearly indistinguishable from the time-decay data. In the fits, $J = 30$ cm^{-1} for all micelles, with $\epsilon_S = 20$, 7, and 4 and $D = 4$, 6, and 7 $Å^2$/ns for DTAB, TTAB, and CTAB, respectively. The differences in the D values are not very significant. In fact, a D value of 5 or 6 $Å^2$/ns could have been used in all calculations without substantially reducing the quality of the fits. These results are summarized in Table 1. Figure 4B shows plots of rate constant vs distance for these parameters. Allowing ϵ_S to vary from one micelle to another makes it possible to fit all of the data with all other parameters being essentially the same, i.e., J, β, and D do not have to vary to describe electron transfer in the three micelles. The variation in ϵ_S produces differences in λ and ΔG, which in turn have a substantial effect on the distance dependence of electron transfer.

The question then arises as to whether it is reasonable to assign different ϵ_S to the headgroup regions of the three micelles. Neutron scattering data have detected regions surrounding the micelles' hydrocarbon cores, with scattering length densities different than the cores, varying in width from 9 to 8 to 7 Å for DTAB, TTAB, and CTAB, respectively.[22,42] The same studies report that the number of methylene groups that have water molecules associated with them is 4, 2.5, and 2.5, for DTAB, TTAB, and CTAB, respectively.[22,42] Both of these results support the conclusion that the surface region of DTAB incorporates more water than the surface region of larger micelles, and that the amount of water in the headgroup region decreases as micelle size increases. One possible explanation is that segments of the surfactant tails near the micelle's surface will want to align with the surface rather than along the micelle's radius to minimize the number of water molecules in contact with the hydrophobic core.[29] However, the methylene units nearest to the ionic headgroup are orientationally hindered.[27] In DTAB this is a larger fraction of the hydrocarbon tail, making DTAB surfactant molecules less capable of achieving the desired exclusion of water.

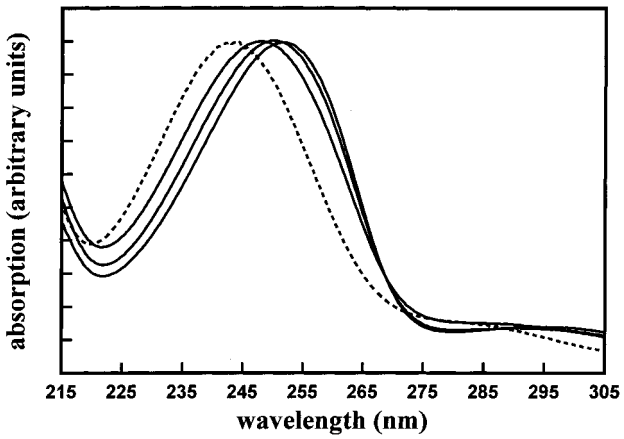

Figure 7. Normalized absorption spectra for DMA in water (dashed line) and in DTAB, TTAB, and CTAB solutions (solid lines from left to right). A distinct shift in peak location is evident from one solution to the next. DTAB spectrum is most water-like, TTAB is intermediate, and CTAB is least water-like.

In addition, spectroscopic experimental evidence supports the idea that the compositions of the headgroup regions of the three types of micelles are different. Figure 7 shows normalized absorption spectra of DMA in water and in the three micelle solutions. As the micelle size increases, there is a significant red shift in the DMA absorption spectrum. The spectra demonstrate that the DMA environment is not the same for the three micelles. The spectra suggest that DMA in the DTAB headgroup region has the most water-like environment and that the headgroup regions of the micelles are less water-like as surfactant chain length increases.

The values obtained for ϵ_S are consistent with decreasing water penetration as micelle radius increases. It is the decreasing water penetration and the accompanying decrease in the headgroup region dielectric constant with increasing micelle size that is responsible for the micelle size dependence of the electron-transfer dynamics. The intent of this paper is to explain the observed size dependence through the application of a detailed theory of λ and ΔG in the heterogeneous micelle systems, rather than to obtain absolutely quantitative values of ϵ_S. Further refinements of the theory by the inclusion of polarization effects are in progress. These may modify the values obtained for ϵ_S and J, but the general conclusions will remain. It should be noted that the value of $J = 60$ cm^{-1} reported in ref 1 was obtained for the three micelles by arbitrarily choosing $\lambda_{contact}$ values. That value of J differs by a factor of

2 from the $J = 30$ cm^{-1} obtained here with the detailed theory. The arbitrary approach did not provide a physical model or values of ϵ_S. The important fact is that the 3-phase model is able to successfully describe data that could not be sufficiently explained by either a continuum model or the 2-phase model. These results demonstrate that electron transfer occurring in the micelle headgroup region must be described with the 3-phase theory using distinct properties for the core, headgroup region, and surrounding water.

V. Concluding Remarks

A theory has been presented for the solvent reorganization energy, λ, and the free energy, ΔG, of electron transfer for a system of donor and acceptors located in the headgroup region of spherical micelles. The theory treats the micelle as a heterogeneous, 3-region system: the micelle core, the headgroup shell, and the surrounding water. Each region has its own dielectric properties. The theory shows that the heterogeneity of the system has a significant impact on λ and ΔG, which in turn substantially change the distance dependence of electron transfer. A simpler 2-region model, a core surrounded by water, also results in significant changes from a homogeneous system. Comparison of the two- and three-region models demonstrates that the headgroup shell plays a substantial role in determining λ and ΔG.

The theoretical results were applied to the analysis of recent experimental data on electron transfer on the surfaces of three micelles which only differ in the length of their surfactant chains. Despite the similarities of the micelles, the experiments show that the electron transfer dynamics vary with micelle size. As the micelle becomes larger, electron transfer is faster. Excellent fits are obtained to the extensive data with physically reasonable values of the relevant parameters. The differences in the electron-transfer rates with micelle size were shown to arise because the headgroup regions of the three micelles have different static dielectric constants. It was argued that the differences in dielectric constants of the headgroup shells arise from different extents of water penetration into the headgroup regions. This explanation is consistent with neutron scattering data[22,42] and spectroscopic data (Figure 7). The theoretical analysis shows that electron transfer is very sensitive to the molecular level details of the micelles' headgroup regions.

Theoretical work is in progress that will add the role of polarization effects to the calculation of λ and ΔG in micelle systems. The addition of polarization effects may change somewhat the values of the parameters reported above, but the overall conclusions should remain unchanged.

Acknowledgment. H.L.T. and M.D.F. would like to thank Dr. Marshall Newton, Brookhaven National Laboratory, for many informative conversations that led to this work. This work was supported by the Department of Energy, Office of Basic Energy Sciences (Grant DE-FG03-84ER13251). H.L.T. thanks the Office of Naval Research for a graduate fellowship. A.V.B. acknowledges a travel grant from the COE project funded by the Science and Technology Agency of Japan.

References and Notes

(1) Weidemaier, K.; Tavernier, H. L.; Fayer, M. D. *J. Phys. Chem. B* **1997**, *101*, 9352.
(2) Marcus, R. A. *J. Chem. Phys.* **1956**, *24*, 966.
(3) Marcus, R. A. *Annu. Rev. Phys. Chem.* **1964**, *15*, 155.
(4) German, E. D.; Kuznetsov, A. M. *Electrochim. Acta* **1981**, *26*, 1595.
(5) Dilonardo, M.; Maestro, M. *Chem. Phys. Lett.* **1991**, *180*, 353.
(6) Perng, B. C.; Newton, M. D.; Raineri, F. O.; Friedman, H. L. *J. Chem. Phys.* **1996**, *104*, 7177.
(7) Spernol, A.; Wirtz, K. *Z. Naturforsch. Teil A* **1953**, *89*, 522.
(8) Rehm, D.; Weller, A. *Isr. J. Chem.* **1970**, *8*, 259.
(9) Fox, M. A. Photoinduced Electron Transfer in Arranged Media. In *Topics in Current Chemistry*; Mattay, J., Ed.; Springer-Verlag: Berlin, 1991; Vol. 159; p 67.
(10) Nakagaki, M.; Komatsu, H.; Tanaka, H.; Handa, T. *Bull. Chem. Soc. Jpn.* **1986**, *59*, 3007.
(11) Hammarström, L.; Berglund, H.; Almgren, M. *J. Phys. Chem.* **1994**, *98*, 9588.
(12) Hubig, S. M. *J. Lumin.* **1991**, *47*, 137.
(13) Lerebours, B.; Chevalier, Y.; Pileni, M. P. *Chem. Phys. Lett.* **1985**, *117*, 89.
(14) Weidemaier, K.; Fayer, M. D. *J. Chem. Phys.* **1995**, *102*, 3820.
(15) Weidemaier, K.; Fayer, M. D. *J. Phys. Chem.* **1996**, *100*, 3767.
(16) Weidemaier, K.; Tavernier, H. L.; Chu, K. T.; Fayer, M. D. *Chem. Phys. Lett.* **1997**, *276*, 309.
(17) Zaloj, V.; Agmon, N. *Chem. Phys. Lett.* **1997**, *270*, 476.
(18) Eriksson, J. C.; Gillberg, G. *Acta Chem. Scand.* **1966**, *20*, 2019.
(19) Hirata, H.; Aoki, S.; Taga, K.; Okabayashi, H.; Yoshida, T.; Kawakatsu, T. *Colloid Polym. Sci.* **1995**, *273*, 1080.
(20) Reiss-Husson, F.; Luzzati, V. *J. Phys. Chem.* **1964**, *68*, 3504.
(21) Matsuoka, H.; Tsurumi, M. *Phys. Rev. B* **1988**, *38*, 6279.
(22) Berr, S. S. *J. Phys. Chem.* **1987**, *91*, 4760.
(23) Briggs, J.; Nicoli, D. F.; Ciccolello, R. *Chem. Phys. Lett.* **1980**, *73*, 149.
(24) Dorshow, R.; Briggs, J.; Bunton, C. A.; Nicoli, D. F. *J. Phys. Chem.* **1982**, *86*, 2388.
(25) Vinson, P. K.; Bellare, J. R.; Davis, H. T.; Miller, W. G.; Scriven, L. E. *J. Colloid Interface Sci.* **1991**, *142*, 74.
(26) Lin, Z.; Cai, J. J.; Scriven, L. E.; Davis, H. T. *J. Phys. Chem.* **1994**, *98*, 5984.
(27) Laaksonen, L.; Rosenholm, J. B. *Chem. Phys. Lett.* **1993**, *216*, 429.
(28) Karaborni, S.; O'Connell, J. P. *J. Phys. Chem.* **1990**, *94*, 2624.
(29) Vacatello, M.; Yoon, D. Y. *J. Chem. Phys.* **1990**, *92*, 757.
(30) Waka, Y.; Hamamoto, K.; Mataga, N. *Chem. Phys. Lett.* **1979**, *62*, 364.
(31) Rothenberger, G.; Grätzel, M. *Chem. Phys. Lett.* **1989**, *154*, 165.
(32) Sano, H.; Tachiya, M. *J. Chem. Phys.* **1981**, *75*, 2870.
(33) Grätzel, M.; Thomas, J. K. *J. Phys. Chem.* **1974**, *78*, 2248.
(34) Grätzel, M. Solar Energy Harvesting. In *Photoinduced Electron Transfer. Part D.*; Fox, M. A., Chanon, M., Eds.; Elsevier: New York, 1988; p 394.
(35) Barzykin, A. V.; Tachiya, M. *Heterog. Chem. Rev.* **1996**, *3*, 105.
(36) Thomas, J. K. *Acc. Chem. Res.* **1977**, *10*, 133.
(37) Gelbart, W. M.; Ben-Shaul, A. *J. Phys. Chem.* **1996**, *100*, 13169.
(38) Lindman, B. Structural Aspects of Surfactant Micellar Systems. In *Surfactants*; Tadros, T. F., Ed.; Academic Press: Orlando, 1984; p 83.
(39) Ben-Shaul, A.; Gelbart, W. M. *Annu. Rev. Phys. Chem.* **1985**, *36*, 179.
(40) Goyal, P. S.; Dasannacharya, B. A.; Kelkar, V. K.; Manohar, C.; Srinivasa Rao, K.; Valaulikar, B. S. *Physica B* **1991**, *174*, 196.
(41) Watanabe, K.; Ferrario, M.; Klein, M. L. *J. Phys. Chem.* **1988**, *92*, 819.
(42) Berr, S.; Jones, R. R. M.; Johnson, J. S. *J. Phys. Chem.* **1992**, *96*, 5611.
(43) Clint, J. H. *Surfactant Aggregation*; Chapman and Hall: New York, 1992.
(44) Din, K.-U.; Kumar, S.; Aswal, V. K.; Goyal, P. S. *J. Chem. Soc., Faraday Trans.* **1996**, *92*, 2413.
(45) Weidemaier, K.; Tavernier, H. L.; Swallen, S. F.; Fayer, M. D. *J. Phys. Chem. A* **1997**, *101*, 1887.
(46) Burshtein, A. I. *Chem. Phys. Lett.* **1992**, *194*, 247.
(47) Dorfman, R. C.; Fayer, M. D. *J. Chem. Phys.* **1992**, *96*, 7410.
(48) Dorfman, R. C.; Tachiya, M.; Fayer, M. D. *Chem. Phys. Lett.* **1991**, *179*, 152.
(49) Purcell, K. F.; Blaive, B. Theory of Electron-Transfer Reactions. In *Photoinduced Electron Transfer: Part A. Conceptual Basis*; Fox, M. A., Chanon, M., Eds.; Elsevier: New York, 1988; p 123.
(50) Bolton, J. R.; Archer, M. D. Basic Electron-Transfer Theory. In *Electron Transfer in Inorganic, Organic, and Biological Systems*; Bolton, J. R., Mataga, N., McLendon, G., Eds.; The American Chemical Society: Washington, 1991; p 7.
(51) Marcus, R. A. *J. Chem. Phys.* **1956**, *24*, 979.
(52) Marcus, R. A. Theory and Applications of Electron Transfers at Electrodes and in Solution. In *Special Topics in Electrochemistry*; Rock, P. A., Ed.; Elsevier: Amsterdam, 1977; p 161.
(53) Kharkats, Y. I. *Electrokhimiya* **1973**, *9*, 881.
(54) Barzykin, A. V.; Tachiya, M. *Chem. Phys. Lett.* **1998**, *285*, 150.
(55) Tachiya, M. *Chem. Phys. Lett.* **1994**, *230*, 491.
(56) Weller, A. *Z. Physik. Chem. NF* **1982**, *133*, 93.

(57) Rice, S. A. *Diffusion-Limited Reactions*; Elsevier: Amsterdam, 1985.
(58) Press, W. H.; Flannery, B. P.; Teukolsky, S. A.; Vetterling, W. T. *Numerical Recipes in C*; Cambridge University Press: Cambridge, 1988.
(59) Nelder, J. A.; Mead, R. *Comput. J.* **1965**, *7*, 308.
(60) Ediger, M. D.; Domingue, R. P.; Fayer, M. D. *J. Chem. Phys.* **1984**, *80*, 1246.
(61) Grätzel, M.; Kalyanasundaram, K.; Thomas, J. K. *J. Am. Chem. Soc.* **1974**, *96*, 7869.
(62) Tanford, C. *J. Phys. Chem.* **1972**, *76*, 3020.
(63) Swallen, S. F.; Weidemaier, K.; Tavernier, H. L.; Fayer, M. D. *J. Phys. Chem.* **1996**, *100*, 8106.
(64) Closs, G. L.; Miller, J. R. *Science* **1988**, *240*, 440.
(65) Gray, H. B.; Winkler, J. R. *Annu. Rev. Biochem.* **1996**, *65*, 537.
(66) Miller, J. R.; Beitz, J. V.; Huddleston, R. K. *J. Am. Chem. Soc.* **1984**, *106*, 5057.
(67) Marcus, R. A.; Sutin, N. *Biochim. Biophys. Acta* **1985**, *811*, 265.
(68) Guarr, T.; McLendon, G. *Coord. Chem. Rev.* **1985**, *68*, 1.
(69) Riddick, J. A.; Bunger, W. B. *Organic Solvents: Physical Properties and Methods of Purification*, 3rd ed.; John Wiley & Sons: New York, 1970; Vol. II.
(70) Nery, H.; Söderman, O.; Canet, D.; Walderhaug, H.; Lindman, B. *J. Phys. Chem.* **1986**, *90*, 5802.
(71) Walderhaug, H.; Söderman, O.; Stilbs, P. *J. Phys. Chem.* **1984**, *88*, 1655.
(72) Eriksson, P.-O.; Khan, A.; Lindblom, G. *J. Phys. Chem.* **1982**, *86*, 387.